International Journal of Control, Automation, and Systems 21(4) (2023) 1127-1142
http://dx.doi.org/10.1007/s12555-021-1095-8
ISSN:1598-6446 eISSN:2005-4092
http://www.springer.com/12555

Active Optimal Roll Control of Railway Vehicles in Curved Tracks Using an Electrically Actuated Anti-roll Bar System

Benyamin Anafjeh, Hassan Moosavi, and Mohammad Danesh*

Abstract: Active tilting control is now one of the technologies utilized widely in high-speed railway vehicles. This paper tries to decrease the lateral acceleration on passengers (caused by high-speed motion in a curve) using an electrical anti-roll bar (ARB) that provides a limited amount of carbody tilt. A dynamic model is employed for a modern railway vehicle with its active anti-roll bar (AARB). Moreover, an attempt is made to design three control approaches of Kalman filter-based Model Predictive Control, Linear Quadratic Gaussian servo control, and proportional-integral regulator in such a way to be robust against noise and simultaneously improve ride comfort and vehicle dynamic performance. The active anti-roll bar acts as an actuator with a brushless DC (BLDC) motor, permitting active tilt control. Finally, the performance of the tilting vehicle and electric actuation system employing different control structures is assessed based on numerical simulations. Furthermore, a helpful comparison is drawn between the optimal and other simulated control approaches concerning ride comfort. The simulation results reveal better competency of Kalman filter-based Model Predictive Control in achieving the reference pursuit plus noise canceling and improving ride comfort.

Keywords: Brushless DC motor, lateral acceleration, LQG servo control, model predictive control, ride comfort, tilt control system, tilting train.

1. INTRODUCTION

The active tilting train is an established method in high-speed railway transportation. These modern railway vehicles are successfully servicing various countries such as Italy, Sweden, and Japan [1]. Moreover, there is a rising interest in the tilting concept for metro systems [2]. The passengers and carbody undergo a lateral force when a train traverses a curve, causing the vehicle body to roll outwards of the curve. In tilting trains, tilting the carbody inwards of the turn reduces the lateral acceleration experienced by passengers. This movement is acted according to a control system encompassing sensors and electronic parts operated by a predominantly hydraulic or electrical system. Such action does not usually influence the safety of the train as long as the transversal position of the carbody center of gravity is not tangibly changed. Of course, the overturn torque is decreased in the turns due to the centrifugal force [3].

There are various mechanisms, including air cushions, hydraulic and pneumatic pistons, to make the vehicle perform such a roll movement (tilting) into the curve. Some researches offered methods for tilting the carbody using hydraulic actuators [4,5]. For instance, the method of tilting bolsters is currently being used extensively. In this case, the tilting bolster is linked to a bogie. Actuators that are placed between the bogie and bolster create a tilting move under the secondary suspension system [6]. In addition, a paper presented an active suspension configuration including a lateral actuator and airsprings that integrates tilt and active lateral secondary suspension control in order to improve the tilt control system efficiency [7]. In an experimental study on tilting bolsters, a hydraulic tilting actuator system was developed. The experiment was conducted employing a proportional-derivative controller on the Korean tilting train [8]. Goodall, Pearson, and Perret proposed one applied approach that uses an active anti-roll bar (AARB) [1]. Originally, the AARB is widely used for passenger comfort and rollover prevention in vehicles [9]. As an example, Vu *et al*. [10] applied an electronic servo-valve hydraulic AARB with the aim of improving the vehicle roll stability. Using an active anti-roll bar with an electrical motor as an electromechanical actuator is deemed an appropriate solution for tilting the train inwards on track corners, leading to the reduction of lateral acceleration and increase of the passenger's comfort. Besides, it works faster than the hydraulic actuator, and it is not accompanied by the hydraulic system breakdown,

Manuscript received December 25, 2021; revised March 30, 2022 and May 17, 2022; accepted June 15, 2022. Recommended by Associate Editor Un-Chul Moon under the direction of Senior Editor Jay H. Lee.

Benyamin Anafjeh, Hassan Moosavi, and Mohammad Danesh are with the Department of Mechanical Engineering, Isfahan University of Technology, University Boulevard, Esteghlal Square, Isfahan, Iran (e-mails: b.anafjeh@alumni.iut.ac.ir, {moosavi, danesh}@iut.ac.ir).
* Corresponding author.

costs, and energy consumption [11]. Although hydraulic actuators are convenient for high-force applications such as carbody tilt, their speed is hard to control accurately, and they may cause delays in tilting action on fast and consecutive curved tracks. On the other hand, electric actuators offer repeatable abilities with ease, and the speed is also quickly controlled and smooth on curved tracks.

Several studies have focused on semi-active and active railway vehicle suspension systems and their effects on dynamic performance and ride quality [12,13]. Nowadays, tilting action in high-speed tilting trains is performed by active control, and clearly, control engineering has contributed to the improvement of active tilting train systems technology. Magalhàes *et al*. [14] obtained a linear model of the tilting system from the linearization of a detailed multi-body model [15] and compared the results of some control algorithms for the tilting system. A recent work presented in [16] employed the H_∞ sensitivity controller on the tilt control, considering the deterministic (curving acceleration response) and stochastic (ride quality on straight track irregularities) trade-off. Another study on deterministic and stochastic trade-off was performed by [5] utilizing PI/PID-type control structures. Hassan *et al*. [17] discussed optimized Ziegler-Nichols PID control on tilt control performance for non-precedent rail vehicle tilt. Today's industrial norm employs an accelerometer on a non-tilting part of the precedent vehicle (or front passenger vehicle) to provide the essential tilting angle. This method is called "tilt with precedence" or "command-driven with precedence" and is more common than "nulling-tilt" or "non-precedent tilt," which uses feedback control from a lateral accelerometer mounted on the carbody. A comparison between these two methods can be found in [7]. The study [18] proposed two control schemes, including a model-based estimation and a robust H_∞ based approach, which is applicable to each vehicle independently, without the need for precedence control. In the present work, the designed control systems use carbody tilt angle feedback to ensure each vehicle rolls to the indicated carbody tilt angle. This feedback might be affected by noise, and such measurement noise can lead to instability issues in the system. The system generates the desired carbody tilt angle using the vehicle speed, information from an onboard track database, and data associated with the desired lateral acceleration perceived by passengers. Thus, the exact location of the vehicle on the track, as well as the curve data stored in the database, must be known. A recent study has focused on rejecting the effects of measurement noise in an AC/DC interconnected system using a Kalman filter [19]. The Kalman filter is an optimal estimator which is easy to calculate and minimizes the error statistically. This filter has the advantage that it is suitable for linear systems, and it can be used widely in practical applications such as high-speed railway vehicles [7]. Another recent research [20] presented an adaptive optimal control approach that might be helpful to achieve the desired disturbance rejection and tracking performance for disturbed tilting train systems. This approach is based on reinforcement learning which can learn both the optimal feedback control gain and the appropriate feedforward control gain utilizing quantifiable data. Implementing this approach on a LCL coupled inverter-based distributed generation system (a linear continuous-time system) showed the good performance of disturbance elimination and reference tracking of this approach.

Despite many studies on controlling tilting vehicles, to the best of our knowledge, no particular research can be found that uses an active electrical anti-roll bar considering the behavior of the electric motor (in this case, Brushless DC Motor) on tilt control. Depending on the control approach, actuators may show different responses, so it is essential that the designed controller causes the actuation system to have an appropriate response in the presence of noises and disturbances. Further, the existence of different stages and changes on a curve leads to variations in the reference signal. Due to the variability of the reference signal, it is essential to ensure that the control system follows the reference command. Linear quadratic regulator (LQR) or the conventional Linear quadratic Gaussian (LQG) controller seems to be a viable solution for these conditions. However, the former may not have proper performance in a noisy system. Besides, the latter lacks the ability of reference tracking since it is designed based on fixed references. Thus, this paper tries to introduce a new control strategy with two main aims: (i) rejecting noises and pursuing the reference command (ii) leading to a proper response of the BLDC motor. To achieve these objectives, LQG servo control and Kalman filter-based model predictive control (MPC-KF) have been used for gaining proper tilting action. In this work, the applied LQG servo controller is developed by incorporating a linear quadratic integrator (LQI) with a Kalman filter.

The LQG servo control and MPC are theoretically similar in respect of the analytical form of the cost function (quadratic weighting plant state) and control signal. However, the techniques applied for the minimization are substantially different. Regarding resolving the tracking issue, The LQI part of the LQG controller has the ability to improve the reference tracking for the system and operates as a suited full state feedback compensator. In addition, the Kalman filter can estimate the unknown states. MPC integrates a prediction strategy and a control algorithm to keep the system output at a reference signal by updating the control signal. Since MPC cannot reject disturbances and measurement noises satisfactorily, it is crucial to use a combined MPC and Kalman filter (MPC-KF) for state estimation and improving disturbance rejection [21,22].

As the second contribution, the present study designs a modified LQG control system and MPC-KF considering the brushless DC motor and assesses their performance

using time-domain (simulation) analysis. As per the best knowledge of the authors, using these two quadratic approaches for carbody tilt control, despite their benefits, has not been reported in the literature. For a deeper assessment of the designed approaches regarding the performance of the electric actuation system, a conventional PI controller is considered, and its results are compared with those of the designed LQG servo and MPC-KF controllers in the presence of measurement noise.

The structure of this paper is as follows: In Section 2, the BLDC motor and ARB are modeled, as well as the tilting railway vehicle. In Section 3, the modified LQG servo control and MPC-KF are designed. The system performance is further analyzed in Section 4. Finally, conclusions are presented in Section 5.

2. MODELING

2.1. Anti-roll bar model

For deriving the relation between motor rotation and deviation angle produced by the actuator, consider Fig. 1. L_1 and L_2 are the bar and arm length, respectively. The geometrical relationship between the rotation angle of the actuator ϕ and the tilting angle of the anti-roll bar δ_a can be expressed by

$$L_2\phi = \frac{L_1}{2}\delta_a \Rightarrow \delta_a = 2\frac{L_2}{L_1}\phi. \tag{1}$$

Considering Fig. 2, F is the force exerted by the anti-roll bar onto the carbody, k_{vr} is the anti-roll bar stiffness, and T is the torque created by the BLDC motor positioned in the midsection of the anti-roll bar. Equation (2) demonstrates the relationship between the tilting angle of the actuator and the torque produced by the motor. B is the force of the two supports.

$$\frac{L_1}{k_{vr}L_2}T = \delta_a. \tag{2}$$

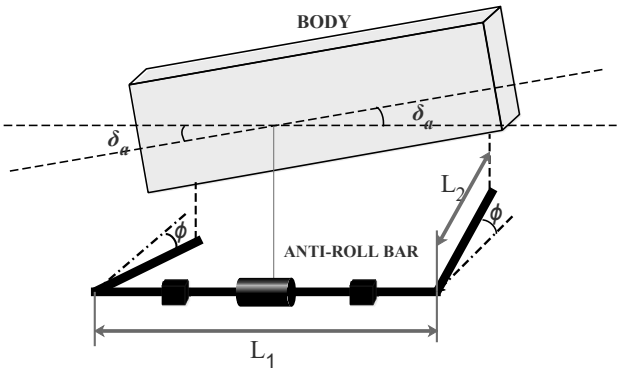

Fig. 1. Scheme of an active anti-roll bar.

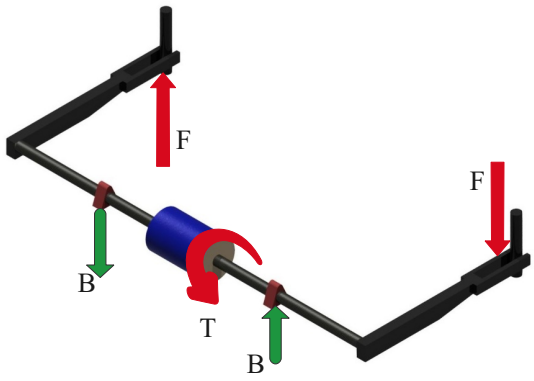

Fig. 2. The electric active anti-roll bar model.

2.2. Model of BLDC motor

Active anti-roll bar includes a brushless DC motor (BLDC) of three-phase trapezoidal type with a reducer gearbox. The type of gearbox is a harmonic or strain wave with a high reduction ratio (e.g., $n_r = 200$) which amplifies the motor torque and brings about a high output torque.

Fig. 3 shows different parts of this electromechanical actuator. It is seen that the No. 2 stabilizer bar is linked to the housing of the actuator. The output shaft of the motor and the No. 1 stabilizer bar are attached to each other. Output torque is transferred in the opposite direction to the No.1 stabilizer bar. A set of essential rotation sensors are provided to control the rotational movement of the motor [23].

A closed-loop speed control system of a BLDC motor consisting of 6 parts is shown in Fig. 4. These six parts include the permanent magnet synchronous motor, the three-phase inverter, the three-phase diode rectifier, the speed controller, the braking chopper, and the current controller. A PI regulator forms the structure of the speed controller. Details of the speed controller are provided in Table 1. The sign "(-)" in the table indicates that the corresponding parameter has no unit. For controlling the speed, the command to the current controller block is a torque setpoint defined based on the PI regulator. The cur-

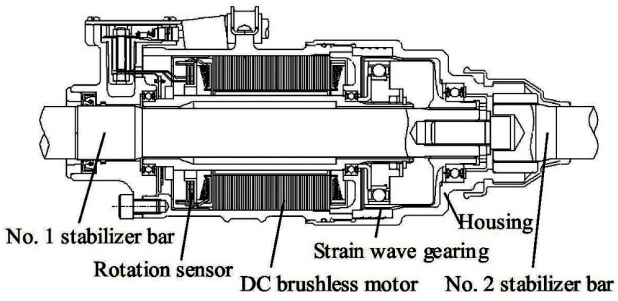

Fig. 3. The electric actuator of active anti-roll bar [11].

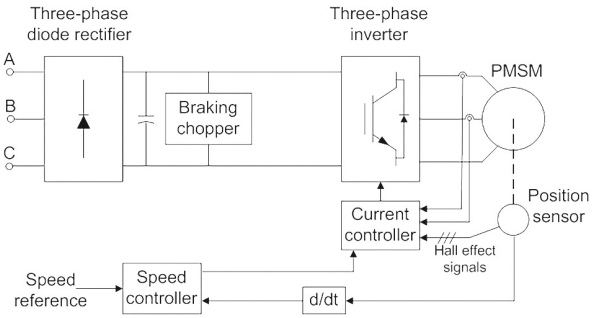

Fig. 4. Closed-loop BLDC motor speed control [24].

Table 1. PI parameters of the speed controller.

Proportional gain	18.64 (-)
Integral gain	7324.7 (s^{-1})
Torque output limit	±600 Nm

rent controller calculates the reference currents concerning the reference torque, and it feeds the motor using a three-phase current regulator [24].

Trapezoidal BLDC motor has a trapezoidal back electromotive force (EMF). The characteristic equations of BLDC motors can be represented as [25]

$$V_{app} = R_s I + L_{SI}\frac{dI}{dt} + e_{emf}, \tag{3}$$

$$T_e = B_f\gamma + J_{rot}\frac{d\gamma}{dt} + T_l, \tag{4}$$

$$T_e = \Lambda_t\left(I_a f(N_p\beta) + I_b f\left(N_p\beta - \frac{2\pi}{3}\right) + I_c f\left(N_p\beta + \frac{2\pi}{3}\right)\right). \tag{5}$$

The relation between the stator phase current and terminal voltage is in the form of (3). The trapezoidal function is shown in Fig. 5. This function depends on rotor position (β) and has a value between -1 and 1, as illustrated in Fig. 5, to show the distribution of back EMF. Periodically the back EMF is fixed for 120° displacement and then varies linearly for 60° displacement. The trapezoidal back EMF of each phase can be obtained by

$$e_a = \Lambda_e\gamma f\left(N_p\beta\right), \tag{6}$$

$$e_b = \Lambda_e\gamma f\left(N_p\beta - \frac{2\pi}{3}\right), \tag{7}$$

$$e_c = \Lambda_e\gamma f\left(N_p\beta + \frac{2\pi}{3}\right). \tag{8}$$

The mechanical output torque of the electric motor can be determined based on (4). Here T_e is the total electromagnetic torque. Equation (5) shows the relationship between the phases currents and electromagnetic torque, where Λ_t is the torque constant. I_a, I_b, and I_c are the phase currents. Table 2 shows the parameters of the BLDC motor.

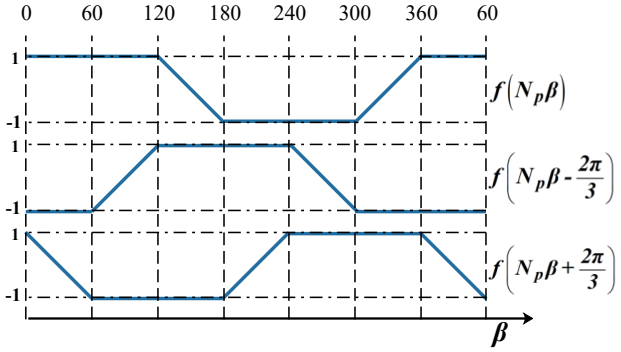

Fig. 5. Trapezoidal function based on the rotor position.

Table 2. Parameters of the BLDC motor.

Parameter	Definition	Value	Unit
V_{app}	Terminal voltage	780	volt
R_s	Stator resistance	0.19	Ω
L_{SI}	Stator inductance	4.6×10^{-3}	H
B_f	Friction constant	0.005	N.m.s
J_{rot}	Rotor inertia	0.116	Kg.m^2
Λ_t	Torque constant	7.15	Nm/Arms
Λ_e	Back EMF constant	442.8	Vrms/krpm
N_p	Number of poles	8	-
I	Stator phase current	-	A
T_l	External load	-	Nm
e_{emf}	Induced back EMF	-	volt
β	Electrical rotor angle	-	rad
γ	Rotor speed		rad/sec
$f(\cdot)$	Trapezoidal shape reference function	-	-

2.3. Mathematical model of tilting vehicle

The model used for design purposes is according to an end-view model of a tilting railway vehicle (Fig. 6), including both lateral and roll dynamics of both the vehicle body and bogie. The airsprings and the bogie lateral kinematics are also included in the modeling phase. For simplicity, wheelset dynamics (interaction between the wheels and rails) are not taken into account in the tilt action and behavior of the secondary suspension. The vertical suspension is represented by the pair of airsprings, which only contribute to the roll motion of the vehicle despite the fact that the vertical degrees of freedom are ignored. The stiffness of an anti-roll bar placed between the carbody and bogie is also depicted in the model. A rotational displacement of the actuator provides the active tilt ($\boldsymbol{\delta}_a$) (assumed to be ideal), in series with the roll stiffness, i.e., the concept of an active anti-roll bar [26].

The end-view model can be represented by (9) to (12) and corresponds to curved track parameters, including R as the curve radius and θ_o as the track cant angle. The airspring model and all parameters/constants/variables are

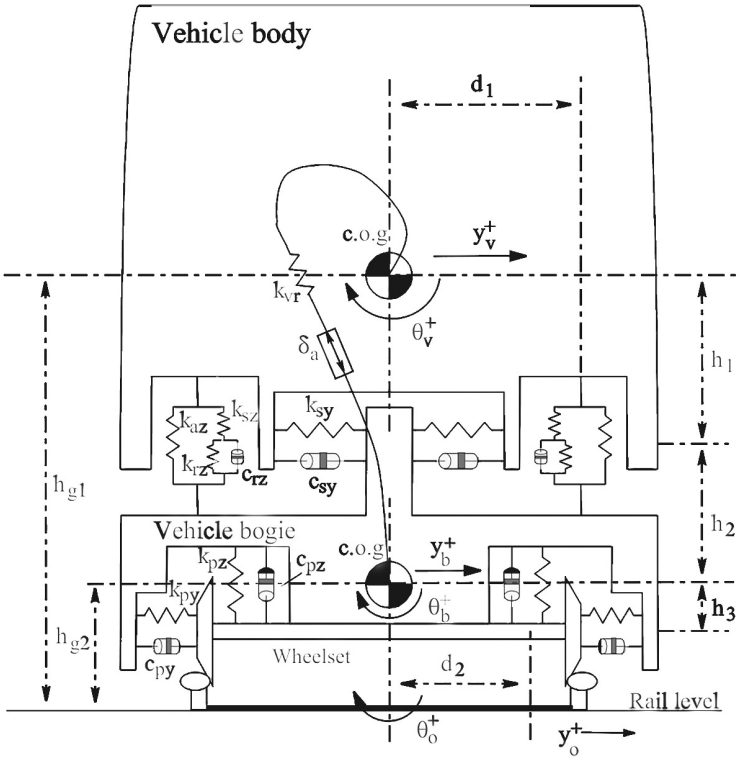

Fig. 6. End-view of a tilting railway vehicle [26].

provided in Appendix A [26]. The motion equations are expressed as

Body lateral dynamics:

$$m_v\ddot{y}_v = -2k_{sy}y_v + 2k_{sy}h_1\theta_v + 2k_{sy}y_b + 2k_{sy}h_2\theta_b - \frac{m_v v^2}{R} + m_v g\theta_o - m_v h_{g1}\ddot{\theta}_o. \quad (9)$$

Body roll dynamics:

$$\begin{aligned} i_{vr}\ddot{\theta}_v = {} & (2h_1k_{sy} + m_v g)y_v \\ & - [k_{vr} + 2h_1^2k_{sy} + 2d_1^2(k_{az} + k_{sz})]\theta_v \\ & - y_b(2h_1k_{sy} + m_v g) \\ & + (k_{vr} + 2d_1^2k_{az} - 2h_1h_2k_{sy})\theta_b \\ & - c_{vr}\dot{\theta}_v + c_{vr}\dot{\theta}_b + 2k_{sz}d_1^2\theta_r - i_{vr}\ddot{\theta}_o + k_{vr}\delta_a. \end{aligned} \quad (10)$$

Bogie lateral dynamics:

$$\begin{aligned} m_b\ddot{y}_b = {} & 2k_{sy}y_v - 2h_1k_{sy}\theta_v - 2(k_{sy} + k_{py})y_b \\ & - 2(h_2k_{sy} + h_3k_{py})\theta_b - 2c_{py}\dot{y}_b \\ & + 2h_3c_{py}\dot{\theta}_b - \frac{m_b v^2}{R} + m_b g\theta_o - h_{g2}m_b\ddot{\theta}_o. \end{aligned} \quad (11)$$

Bogie roll dynamics:

$$\begin{aligned} i_{br}\ddot{\theta}_b = {} & 2h_2k_{sy}y_v \\ & + \left[k_{vr} - 2h_2h_1k_{sy} + 2d_1^2(k_{az} + k_{sz})\right]\theta_v \\ & - 2[h_2k_{sy} - h_3k_{py}]y_b \\ & - \left[\begin{matrix} k_{vr} + 2h_2^2k_{sy} + 2h_3^2k_{py} + 2d_2^2k_{pz} \\ + 2d_1^2k_{az} \end{matrix}\right]\theta_b \\ & + 2h_3c_{py}\dot{y}_b - \left(2d_2^2c_{pz} + 2h_3^2c_{py}\right)\dot{\theta}_b \\ & - 2k_{sz}d_1^2\theta_r + 2h_3k_{py}y_o - 2h_3c_{py}\dot{y}_o \\ & - i_{br}\ddot{\theta}_o - k_{vr}\delta_a. \end{aligned} \quad (12)$$

Equation (10) includes an end moment effect $m_v g(y_v - y_b)$, arising from the lateral movement of the body center of gravity. This term shows the effect of body weight and is neglected in (12) due to the high stiffness of the primary suspensions. Clearly, the mathematical model indicates a substantial coupling between the lateral and roll motions, which causes complexity in the system [26]. The lateral acceleration felt by the passengers can be calculated based on Fig. 6 as

$$\ddot{y} = \frac{v^2}{R}\cos(\theta_o + \theta_b + \theta_v) - g\sin(\theta_o + \theta_b + \theta_v). \quad (13)$$

For system analysis and control design purposes, these equations can be expressed in the noisy state-space form with the state vector $\boldsymbol{x}$. Additive terms of process disturbances ($\boldsymbol{\omega}$) with measurement noise ($\boldsymbol{\upsilon}$) in practice are considered. In this model, there would be nine state variables. In (14), the control input denoted by $\boldsymbol{u}$ is the tilting angle of AARB. The measurable system output is $\boldsymbol{\xi}$ which includes carbody roll angle.

Furthermore, $\mathbf{\Pi}$, $\mathbf{\Phi}$, and $\mathbf{\Psi}$ are the state matrix, control input gain matrix, and output matrix, respectively. The plant noise gain matrix is shown by $\mathbf{\Gamma}$. The formation of these matrices can be obtained from (9)-(12). In this study, $\boldsymbol{\upsilon}$ is considered as white Gaussian noise with zero mean ($\boldsymbol{E}(\boldsymbol{\upsilon}) = \mathbf{0}$).

$$\dot{x} = \Pi x + \Phi u + \Gamma \omega, \tag{14}$$

$$\xi = \Psi x + \upsilon, \tag{15}$$

where

$$x = \left[y_v \;\; \theta_v \;\; y_b \;\; \theta_b \;\; \dot{y}_v \;\; \dot{\theta}_v \;\; \dot{y}_b \;\; \dot{\theta}_b \;\; \theta_r \right]^T,$$

$$u = \delta_a,$$

$$\omega = \left[\tfrac{1}{R} \;\; \theta_o \;\; \dot{\theta}_o \;\; \ddot{\theta}_o \;\; y_o \;\; \dot{y}_o \right]^T.$$

It is assumed that the covariance matrices of $\boldsymbol{\upsilon}$ and $\boldsymbol{\omega}$ are V_n (1×1 matrix) and $\boldsymbol{W_n}$ (6×6 matrix).

$$E(\upsilon \upsilon^T) = V_n, \tag{16}$$

$$E(\omega \omega^T) = W_n. \tag{17}$$

In this study, $\boldsymbol{V_n}$ and $\boldsymbol{W_n}$ are selected as below

$$W_n = \mathrm{diag}(2.1 \times 10^{-7},\ 2.23 \times 10^{-3},\ 5.4 \times 10^{-4},\ 0,\ 0,\ 0),$$

$$V_n = 0.10.$$

Here, $\boldsymbol{V_n}$ is based on the designer choice, and main diagonal entries of $\boldsymbol{W_n}$ is obtained through calculating the covariance of R^{-1} & θ_o, their first derivatives, and their second derivatives, respectively.

Before designing any control system, the behavior of the train must be first achieved in inactive mode. For this purpose, the recent obtained equations are employed. Since the simulation is associated with inactive suspension, the actuator displacement $\boldsymbol{\delta}_a$ is zero.

Deterministic track features are used in the simulation to study the vehicle model. The deterministic track consists of 3 segments, including straight, transient, and steady-state. The deterministic track is a curved track with a radius R of 1000 m and a maximum track cant angle (θ_o) of 6 degrees, with a transition length of 108 m at the start and end of the steady-state part (see Fig. 7). It is noteworthy that track cant and track curvature (R^{-1}) rates increase or decrease linearly during the curve transitions. In addition, a nominal vehicle curving speed (v) of 162 km/h is assumed. The results of the simulation in the passive mode are shown in Fig. 8.

Stochastic track irregularities are included in the model as a uniformly distributed random signal which is added to the track cant angle. This random signal is limited to ± 0.6 deg. These track features are typically hard to measure and some data can be obtained through a recorded track database or a particular track condition measurement vehicle. In this work, the track irregularity is mainly based on

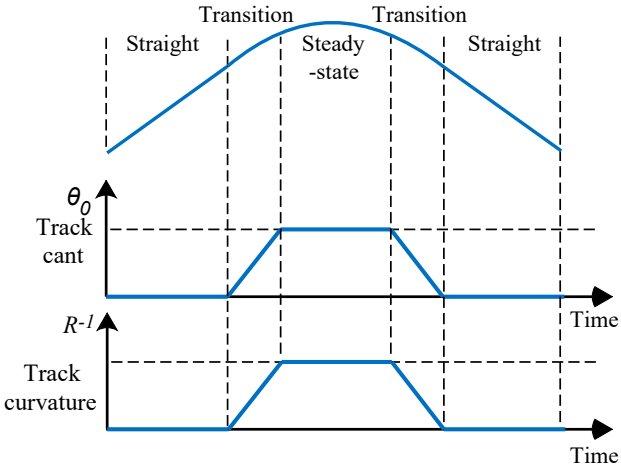

Fig. 7. Representation of deterministic track profile.

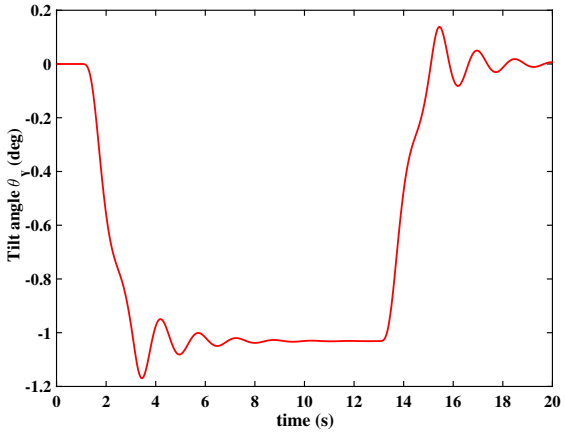

(a)

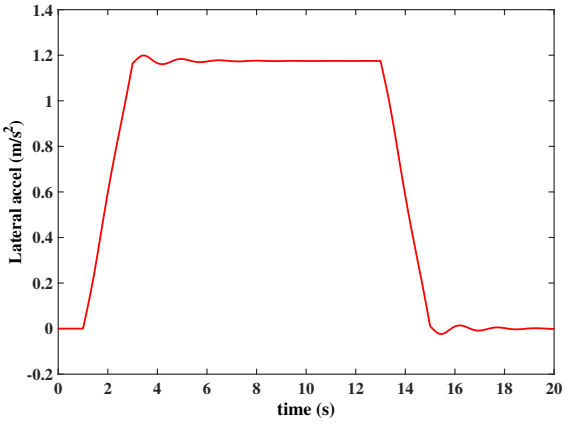

(b)

Fig. 8. Passive (non-tilting) vehicle at 162 km/h. (a) Carbody tilt angle. (b) Lateral acceleration felt by passengers.

random irregularity data, which can be reflective of track defects on high-speed lines.

It is seen that when the vehicle enters the curved track, the carbody begins to roll outwards (negative values of the roll angle) owing to the centrifugal force. Moreover, considering Fig. 8, the lateral acceleration is nearly 1.18 m/s^2, as expected. Based on the figures, the tilting angle and lateral acceleration of the carbody increase due to entering the curve, followed by an elevation in the track cant. Proportionately, the lateral acceleration and the tilting angle of the carbody become zero when the train exit the curved part of the track. The following section presents the design of a set of controllers.

3. CONTROL STRATEGIES

The goal of the tilt control system has been discussed previously. It is noteworthy that this section aims to adopt the model derived from the previous section to design an effective controller. From a control system viewpoint, this can be interpreted as tracking a reference carbody tilt angle that is specified based on the curve geometry and the vehicle speed. The equation for generating body roll angle command (18) is derived based on (13) and defined on the basis of vehicle speed and curve geometry. It is assumed that the angles θ_o, θ_v, and θ_b are small enough, so "small-angle approximation" can be used to derive this relation.

Here θ_v^d and $\ddot{y}^d$ are body roll angle reference and desired lateral acceleration felt by passengers, respectively. In this paper, a 30 percent reduction in non-tilting lateral acceleration is considered to specify the ideal lateral acceleration perceived by the passengers $\ddot{y}^d$ on curves.

$$\theta_v^d = \frac{v^2}{gR} - \frac{\ddot{y}^d}{g} - \theta_o. \tag{18}$$

The maximum carbody tilt angle considered for this application is 2 degrees; in addition, the maximum permitted lateral suspension deflection is subject to the constraint of ± 60 mm before reaching bump stops which prevents excessive motion of the carbody. This value is within the allowed range for overturning issues. This section will prove how the designed control strategies adapt to achieve the control goals; it starts from designing the PI regulator and proceeds to the LQG servo control and MPC-KF designs. As illustrated in Figs. 9 and 10, the control systems are cascade systems that consist of an inner loop with the actuator controller and an outer loop with the secondary suspension roll angle controller. The inner control loop is designed to guarantee that the desired rotor position angle and rotor speed are achieved. Meanwhile, the outer control loop design takes the generated body roll angle into account to improve ride comfort. The details of controlling AARB (inner loop) were clarified in Subsection 2.2.

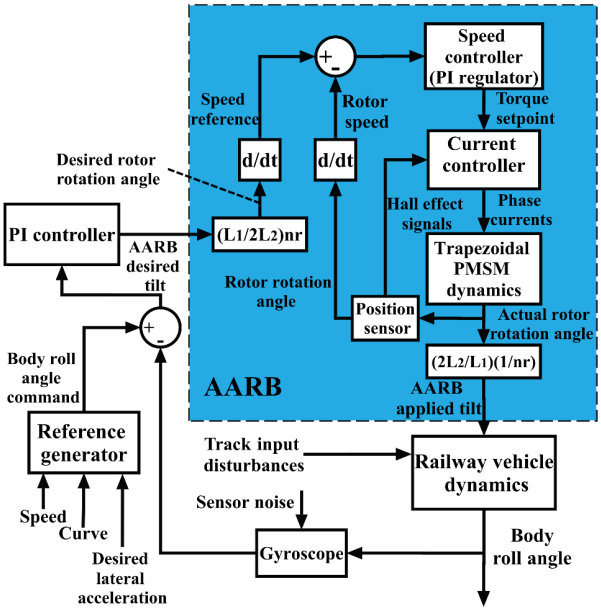

Fig. 9. Block diagram of the closed-loop control system using the Proportional Integral controller and considering the AARB control system in the presence of sensor noise.

Table 3. PI parameters and step response characteristics.

Kp : 38.24 (-)	Ki : 27.36 (s^{-1})
Overshoot: 43.1%	Rise time: 0.019 s

3.1. PI control design

PID is usually the most straightforward popular controller that can be used for active tilting control applications. It provides all three proportional, integral, and derivative actions. The first forces the required amount of acceleration reduction on the steady section of the curved track, and other components can limit phase-lag at high frequencies.

In this section, the derivative contribution is unnecessary because it amplifies high-frequency noise. The main aim of the PI control system is to follow the reference carbody roll angle θ_v^d generated based on the desired lateral acceleration, vehicle speed, and the geometry of the curve being negotiated (see Fig. 9). In this paper, the proportional and integral coefficients can be tuned to minimize the overshoot in the system step response. Moreover, a constraint is applied for the rise time to be less than 0.02 s. The chosen set of parameters from the tuning procedure is listed in Table 3.

3.2. LQG servo control design

The forthcoming section applies the LQG control system to curb and reduce the lateral acceleration of the tilting train in turns. The LQG servo controller is designed with a Kalman filter and an LQI tracker to estimate vari-

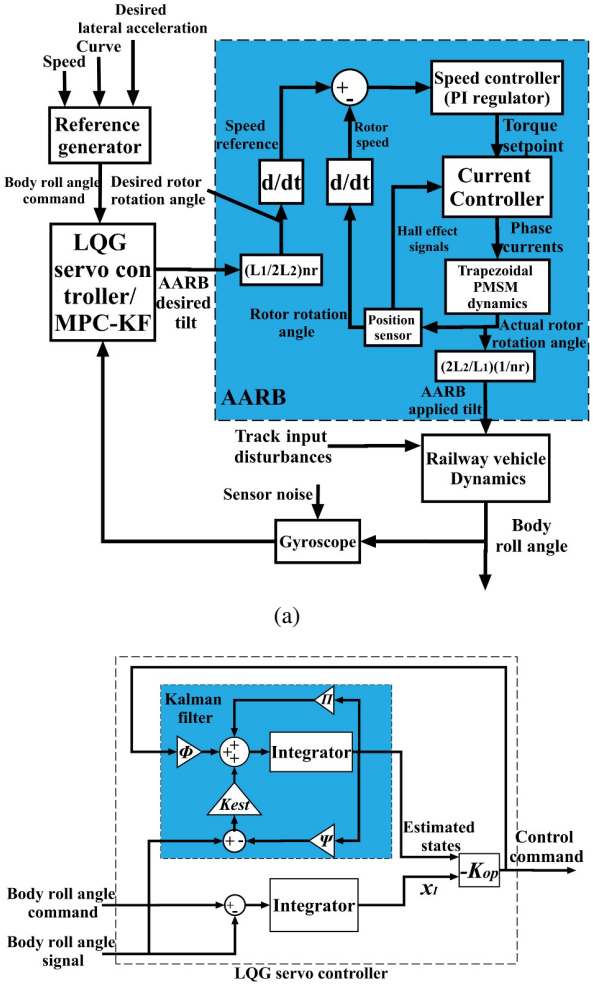

Fig. 10. Block diagram of the control system using the LQG servo controller or MPC-KF. (a) The overall closed-loop system considering the AARB control system and sensor noise (MPC-KF denotes the MPC controller and an accompanying built-in Kalman filter). (b) The modified LQG servo controller structure including the Kalman filter and LQI module.

ables and ensure a suitable reference signal tracking on the control system. The LQI tracker consists of an integrator and a separate gain added to the LQG servo control. In reality, the measurement of all state variables is not a cost-effective and feasible task. For example, when a sensor gives too many noisy results, the system state must be estimated from the output data to implement the state feedback. The Kalman filter estimator acts as an optimal state observer and a low-pass filter, then can reject the process and measurement noises. Fig. 10 exhibits the overall control system block diagram. The inputs of the LQI tracker are reference and feedback signals. As shown, the modified LQG approach associates the outputs of the Kalman filter and LQI with optimal gain matrix $\boldsymbol{K_{op}}$ in (19) in order to provide control command $\boldsymbol{u}$.

$$K_{op} = \begin{bmatrix} K_f & -K_I \end{bmatrix}. \tag{19}$$

The state-feedback controller output is in the form of $\boldsymbol{u} = -\boldsymbol{K_{op}}\boldsymbol{z} = -\boldsymbol{K_{op}}[\hat{\boldsymbol{x}}\ \boldsymbol{x_I}]^{\mathrm{T}}$, where $\boldsymbol{x_I}$ is the integration of the difference between the measured system output $\boldsymbol{\xi}$ and the reference command $\boldsymbol{r}$ defined by (18) and $\hat{\boldsymbol{x}}$ is the estimated variables.

$$x_I = \int (r(t) - \xi(t))dt. \tag{20}$$

The following can be obtained by replacing $\boldsymbol{\xi}(t)$ with (15).

$$\dot{x}_I = r - \Psi x - \upsilon. \tag{21}$$

In order to analyze the whole closed-loop system, new expressions using (19), (14), and (15) can be obtained

$$\begin{bmatrix} \dot{x} \\ \dot{x}_I \end{bmatrix} = \Pi_I \begin{bmatrix} x \\ x_I \end{bmatrix} + \Phi_I \begin{bmatrix} u \\ r \end{bmatrix} + \begin{bmatrix} \Gamma & 0 \\ 0 & -\mathrm{I} \end{bmatrix} \begin{bmatrix} \omega \\ \upsilon \end{bmatrix}, \tag{22}$$

$$\xi = \Psi_I \begin{bmatrix} x \\ x_I \end{bmatrix} + \begin{bmatrix} 0 & -\mathrm{I} \end{bmatrix} \begin{bmatrix} \omega \\ \nu \end{bmatrix}. \tag{23}$$

The matrices as mentioned above are given as

$$\Pi_I = \begin{bmatrix} \Pi & 0 \\ -\Psi & 0 \end{bmatrix},\ \Phi_I = \begin{bmatrix} \Phi & 0 \\ 0 & \mathrm{I} \end{bmatrix},\ \Psi_I = \begin{bmatrix} \Psi & 0 \end{bmatrix}.$$

The optimal state-feedback matrix $\boldsymbol{K_{op}}$ can be obtained by (25). $\boldsymbol{J(u)}$ is the quadratic cost function which state feedback law minimizes this function. $\boldsymbol{P_k}$ is the solution of the control algebraic Riccati equation.This equation requires $\boldsymbol{Q_w}$ and $\boldsymbol{R_w}$ as weighting matrices for calculating $\boldsymbol{P_k}$. $\boldsymbol{Q_w}$ is a symmetric positive semi-definite, and $\boldsymbol{R_w}$ is a symmetric positive definite matrix. These weighting matrices have been selected based on the viewpoint of the controller designer as follows:

$$Q_w = \begin{bmatrix} 0.1 & 0 & 0_{1\times 7} & 0 \\ 0 & 1000 & 0_{1\times 7} & 0 \\ 0_{7\times 1} & 0_{7\times 1} & 0.1 * \mathrm{I}_7 & 0_{7\times 1} \\ 0 & 0 & 0_{1\times 7} & 1000 \end{bmatrix},$$

$$R_w = 1,$$

$$J(u) = \int_0^{\infty} \left(z^T Q_w z + u^T R_w u\right) dt, \tag{24}$$

$$\Pi_I^T P_k + P_k \Pi_I + Q_w - P_k \Phi_I R_w^{-1} \Phi_I^T P_k = 0, \tag{25}$$

$$K_{op} = R_w^{-1} \Phi_I^T P_k. \tag{26}$$

The state-space equation of the Kalman filter is noted in (27). Here $\boldsymbol{K_{est}}$ is the Kalman filter gain. Noting that the matrices $\boldsymbol{\Pi}$, $\boldsymbol{\Phi}$, and $\boldsymbol{\Psi}$ were described in (14) and (15).

$$\dot{\hat{x}} = \Pi \hat{x} + \Phi u + K_{est}(\xi - \Psi \hat{x}). \tag{27}$$

In Fig. 10, it can be observed that the optimal state estimation gain $\boldsymbol{K_{est}}$ can create full state feedback utilizing estimated variables $\hat{\boldsymbol{x}}$. This gain could be calculated using the equation illustrated in (29). Where solving the filter algebraic Riccati produces $\boldsymbol{P_e}$ as a positive semi-definite matrix [27]. Besides, $\boldsymbol{W_n}$ and $\boldsymbol{V_n}$ were mentioned in (16) and (17).

$$\Pi P_e + P_e \Pi^T + \Gamma W_n \Gamma^T - P_e \Phi^T V_n^{-1} \Phi P_e = 0, \tag{28}$$

$$K_{est} = P_e \Phi^T V_n^{-1}. \tag{29}$$

As mentioned earlier, the measurement noise is perceived as white Gaussian noise. This noise affects the gyroscope output in measuring the tilting angle of the body.

3.3. MPC-KF control design

The goal of MPC is to calculate a future control sequence over a specific prediction horizon so that the plant output prediction is closer to the desired output. The block diagram of the MPC is illustrated in Fig. 10. MPC adapts the control signal to meet the objectives while staying within the control constraints, which can be considered as the main superiority of MPC over other optimal control systems, e.g., LQG controller. In MPC design, the control and state signals can be subjected to amplitude and rate constraints. MPC begins predicting future control action by selecting appropriate control horizon M, prediction horizon p, and control-weighting factor $\boldsymbol{\lambda}$. The discretized model of the system is

$$x(k+1) = \Pi_d x(k) + \Phi_d u(k) + \Gamma_d \omega(k), \tag{30}$$

$$\xi(k) = \Psi_d x(k) + \upsilon(k), \tag{31}$$

where $\boldsymbol{\upsilon}(k)$ is the measurement noise assumed to be white noise. The controller contains a built-in steady-state Kalman filter which estimates the current states from the available measurements. In practice, these measurements can be affected by noise, and this issue is considered in this study. In order to estimate the states, a Kalman filter is used with the general form of

$$\hat{x}(k \mid k) = \hat{x}(k \mid k-1) + L_{est}(\xi(k) - \hat{\xi}(k)), \tag{32}$$

$$\hat{\xi}(k) = \Psi \hat{x}(k \mid k-1). \tag{33}$$

Control actions are calculated by minimizing the quadratic objective function at time step k, which can be simply defined as

$$J = \min_{\Delta u} \sum_{i=0}^{p-1} \Big\{ \sum_{j=1}^{n_\xi} \lambda_{i+1,j}^{\xi} (\xi_j(k+i+1 \mid k) - r_j(k+i+1))^2 + \sum_{j=1}^{n_u} \lambda_{i,j}^{\Delta u} \Delta u_j(k+i \mid k)^2 \Big\}, \tag{34}$$

where $\boldsymbol{\lambda_{i,j}^{\xi}}$ is the weight for output j ($j = 0, \ldots, n_\xi$), $\boldsymbol{\lambda_{i,j}^{\Delta u}}$ is the rate weight for control action j at i step ($i = 0, \ldots, p-1$) ahead from the current step. $\boldsymbol{r_j(i)}$ is the reference at time step i. n_ξ and n_u are the number of outputs and control signals, respectively. The regulation of control signal j at time step $k+i$ based on the measurements at time step k is indicated by $\boldsymbol{\Delta u_j(k+i \mid k)}$. Finally, the control action applied to the system can be expressed as

$$u(k) = u(k-1) + \Delta u(k \mid k), \tag{35}$$

The weights in the controller design determine the trade-offs and represent the priority of the related variables to the system's overall performance. The parameters M and p can be used for the tuning of MPC. A larger M enhances the results of MPC at the cost of more calculations [28]. The prediction horizon p is the most important design parameter in terms of control performance and computation time. p is typically assigned long enough to encompass the steady-state effects of all computed future control actions [28]. Despite performance improvement, the computation time increases by enlarging the prediction horizon. To establish a fair balance between calculation time and system performance, p, M, and sampling time are set to be 5, 2, and 0.05 s, respectively. The chosen sampling rate is fast enough for online control of the BLDC motor system. Overall, the chosen sampling rate is fast enough in order that the sampled output of the system captures the system full behavior. The weights on the output variable ($\boldsymbol{\lambda_{i,j}^{\xi}}$) and the control action rate ($\boldsymbol{\lambda_{i,j}^{\Delta u}}$) are 3.60 and 0.028, respectively. The Kalman gain L_{est} is calculated as

$$L_{est} = [-0.18 \;\; 1.21 \;\; -0.18 \;\; 1.67 \;\; 6.5 \;\; 12.67 \;\; 5.79 \;\; -19.73 \;\; 2.26 \;\; 0.5\,]^T.$$

The optimization problem is solved by a quadratic optimization solver based on the KWIK algorithm [29]. In order to achieve the constraints, in addition to the foregoing restriction, it is assumed that the control signal is bounded and the operating range of the ARB (δ_a) is 3 degrees. The constraints on the outputs and control input are presumed to be hard and soft constraints, respectively. Besides, adding the constraint condition can increase MPC solver computation speed which is essential for high-speed movement situations [30]. In summary, the constraints are

$$u^{\text{low}} = -3.5 \text{ deg and } u^{\text{high}} = +3.5 \text{ deg},$$

$$\Delta u^{\text{low}} = -0.5 \text{ deg and } \Delta u^{\text{low}} = +0.5 \text{ deg},$$

$$\theta_v^{\text{low}} = -6 \text{ deg and } \theta_v^{\text{high}} = +6 \text{ deg}.$$

4. RESULTS

This section reports the results of simulations for all three the designed LQG, MPC-KF, and PI controllers concerning the railway vehicle system in the presence of mea-

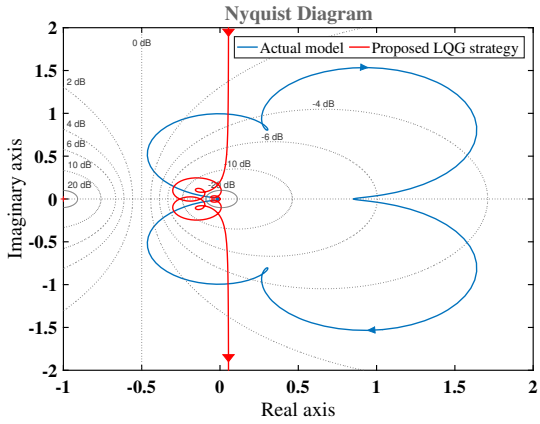

Fig. 11. Nyquist diagram for the model and the LQG servo controller.

surement noise. It is worth noting that the role of the electromechanical actuator is considered in the control system in all of the following simulations.

Firstly, a numerical simulation study using an ideal deterministic track input (without above-mentioned stochastic track irregularity) is conducted for PI, MPC-KF, and LQG servo controllers presented in Section 3 to compare their performance. The vehicle parameters and the characteristics of active electric suspension for this assessment were mentioned in the previous sections and Appendix A. In addition, the curve geometry has the same specification considered in Subsection 2.3. The results of this simulation are presented in Figs. 11-17.

At first, Fig. 11 provides the Nyquist diagram of the closed-loop model. This diagram makes a graphical contribution to predicting the stability of a dynamic system by the open-loop frequency response and open-loop pole location. The Nyquist criterion is broadly used for analyzing systems with feedback control loops. It is conclusive from Section 2 and model descriptions in (12) that the open-loop system has no unstable poles. Moreover, from Fig. 11, it is observed that the number of encirclements of the critical point $(-1, 0)$ is zero for both the studied model and the LQG servo controller. These two criteria indicate the stability of the closed-loop system according to the stability criterion of Nyquist, i.e., if the open-loop system has $\boldsymbol{P}$ unstable poles, the closed-loop system is stable if and only if the Nyquist plot encircles point $(-1,0)$ $\boldsymbol{P}$ times in a counter-clockwise direction.

According to Fig. 10 of Subsection 3.2, the LQG servo and MPC controllers contain a Kalman filter estimator to anticipate all states of the control system when there is noise. Fig. 12 demonstrates the variation of carbody roll angle (θ_v) and its estimation employing the modified LQG and MPC-KF approaches, where the feedback signal is affected by a white Gaussian noise with a power of 10^{-7} and a sample time of 0.1 s. The "Actual" term refers to the case

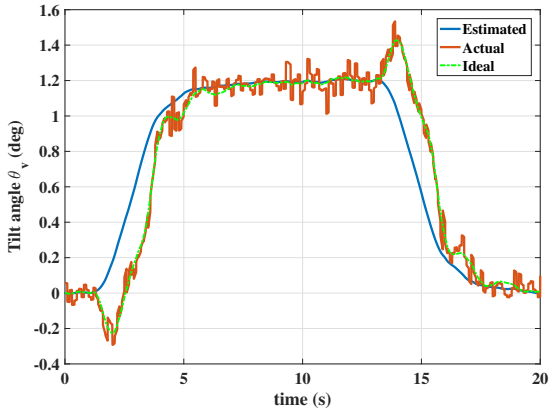

(a)

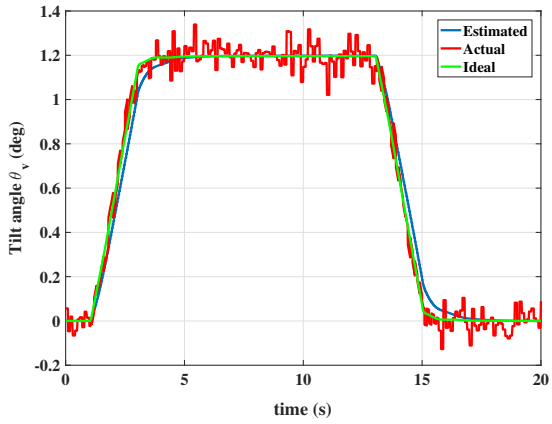

(b)

Fig. 12. Variation of actual and estimated carbody roll angle using the designed (a) LQG servo controller and (b) MPC-KF. "Actual" corresponds to the plant considering noise; "Ideal" corresponds to the plant without considering any noise.

that the measurement noise exists and the "ideal" term corresponds to the measurement noise free case. As Fig. 12 shows, both the LQG servo control and MPC represent an appropriate response during the transient and steady-state sections of the track in the estimation process. In these sections, the variables have been estimated successfully despite the existence of measurement noise, and the level of measurement noise suppression is acceptable. However, as it can be observed from Fig. 13, the Kalman filter associated with MPC provides a more precise dynamic response in the estimating process compared to the modified LQG method. The designed Kalman filter of LQG servo control estimates θ_v with a delay time in contrast with that of MPC-KF. This matter indicates the superiority of MPC-KF over the modified LQG control in terms of estimation error. This delay time will be justified in the following.

Fig. 14 compares the lateral acceleration profile asso-

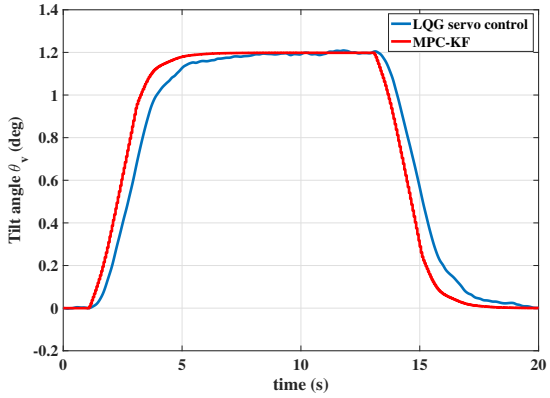

Fig. 13. Comparison of the estimated carbody tilt angle θ_v by the Kalman filters associated with the modified LQG control and MPC-KF.

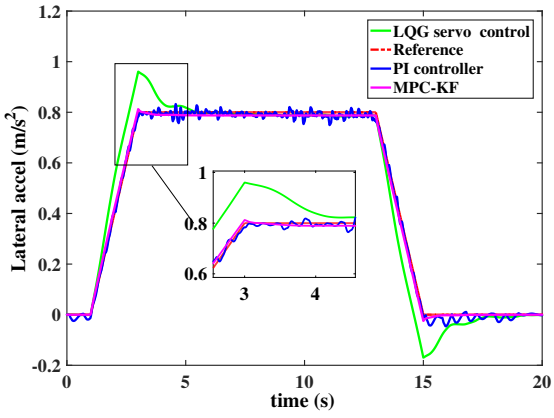

Fig. 14. Evaluating different controllers in the tracking reference.

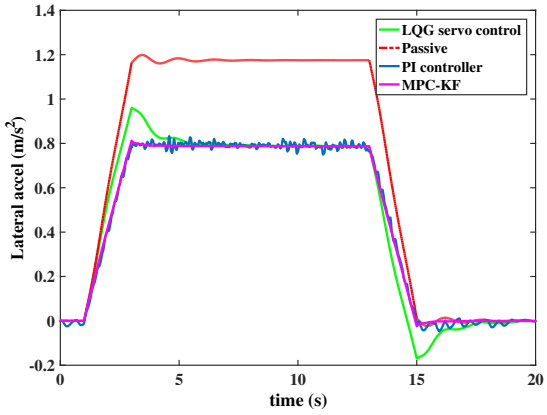

Fig. 15. Lateral acceleration for the different controllers.

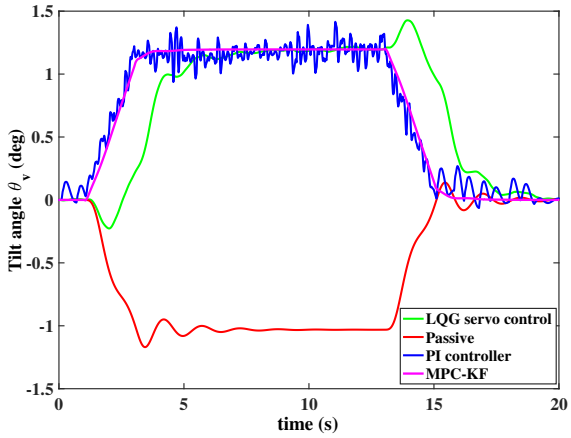

Fig. 16. Carbody roll angle for the different controllers.

ciated with the PI controller with those of the MPC and LQG servo controllers considering the reference and actual state of the system. The reference signal is depicted as a red dotted line. Both the designed optimal controllers performed well in terms of reference tracking. However, there are clear pronounced overshoots with the LQG servo controller at the beginning and end of the steady-state stage of the curve. Despite the presence of noise, it is observed that the LQI part of the LQG structure can keep the output tracking the target signal. It is observed that the designed MPC-KF exhibits a lower settling time, and although the response of the modified LQG controller is still acceptable, it is slower overall. Besides, it is evident that the response of the PI controller contains many slight fluctuations around the command signal $\boldsymbol{r}$, while it achieved the target on reference tracking with reasonable accuracy. Overall, the MPC-KF produces the best performance in terms of reference tracking and noise rejection.

Fig. 15 compares the lateral acceleration profile concerning two vehicle structures: the passive and the active vehicle taking into account three control approaches. It is observed that the lateral acceleration is reduced to the intended value by tilting the vehicle body. As it is clear, the LQG servo control and MPC-KF have properly rejected noise effects on the output. Nonetheless, as expected, measurement noise has affected the lateral acceleration perceived by passengers in the PI controller. Fig. 16 presents a comparison between the carbody roll responses obtained by the PI, MPC-KF, and LQG servo controller. Regarding the time history of the carbody roll rotation of PI controller, the dynamic fluctuations related to the noise are more amplified than the lateral acceleration response. Due to the minor delay in the roll angle response, the lateral acceleration initially follows the uncompensated profile before being appropriately compensated when it reaches the steady curve.

Fig. 17 shows the control signals of the MPC-KF and LQG based controllers. In the case of MPC-KF, since the controller must achieve the defined constraints, as shown in the figure, the control signal is constrained to its limit.

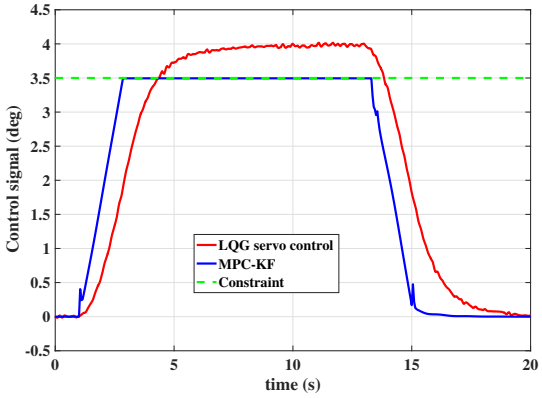

Fig. 17. Control signal for the cases of the modified LQG and MPC-KF.

The green line depicts the defined constraint on the control signal. However, the modified LQG control is free from constraint. In this scenario, a 50 percent reduction in non-tilting lateral acceleration is demanded to evaluate the performance of controllers in terms of satisfying the constraint on the control input.

The obtained optimal gain in the LQG servo controller is not time-varying. On the other hand, regarding MPC based controller, the "gain" is permitted to change during the time, and where possible, a higher gain can be used to improve the performance. The LQG controller naturally selects a small gain to keep the control signal bounded, and consequently, it may increase the controller response time.

In the case of the modified LQG controller, a delay is seen in the control signal at the start of the transient sections of the curve. Because, as the train enters the curve, the error of body roll angle θ_v is slight and hence the gain in the controller is small, the force generated by the actuator is not sufficient compared to the lateral force in order to tilt the carbody inwards the turn. After the error increases, the generated torque can overcome the lateral force and lean the carbody inwards the turn. This matter also occurs at the end of the steady-state section of the curve. Whereas, this occurrence is not seen in the response of MPC-KF due to the varying gain, which can compensate for the delay. In the case of the PI controller, large selected proportional gain reduces the time delay.

As stated before, controller assessment is also related to how the actuator would effectively operate on the curved track. Fig. 18 reports the performance of the electric motor, which determines the torque and the stator current of the BLDC motor. As concerns the behavior of the electromechanical actuator, it can be seen that when the vehicle enters the curve, the torque begins to increase, and at the end of the turn, it reaches zero. Regarding the motor current and torque in Fig. 18, the PI controller shows

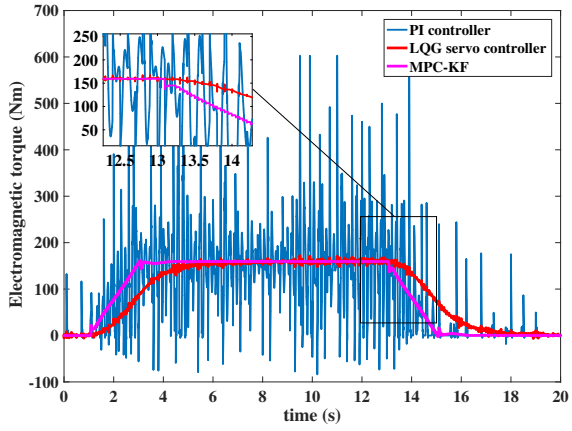

(a)

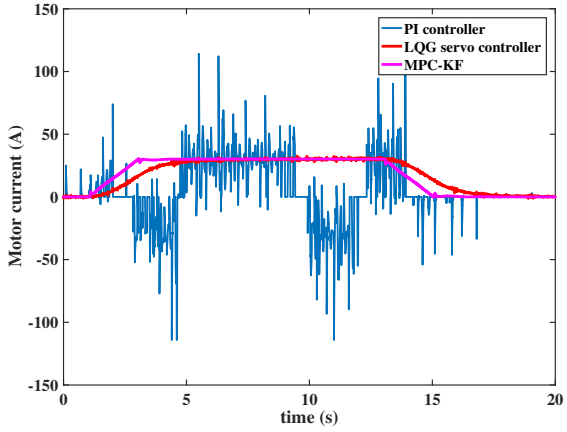

(b)

Fig. 18. Performance of BLDC motor in various controllers. (a) Electromagnetic torque and (b) motor current.

a poor performance due to high-frequency oscillations of electromagnetic torque in the BLDC motor. However, employing the modified LQG control and MPC-KF schemes leads to a decent function of the BLDC motor since such controllers provide an acceptable torque response and can remove noise better (due to using the Kalman filter). In terms of the current response, both the LQG servo and MPC-KF controllers have a more appropriate electrical response compared with the PI controller. Considering the PI controller instead, it is apparent that the stator current amplitude and frequency are high and might be destructive for the motor.

For thoroughness, a sample of the carbody acceleration profile stimulated by the integrated rail track is presented here, i.e., the behavior excited by both deterministic curved track and track irregularities, shown in Fig. 19. It is demonstrated that the designed control approaches have no effect on the stochastic behavior of the tilt vehicle. It is also worth noting that the tilt control system will re-

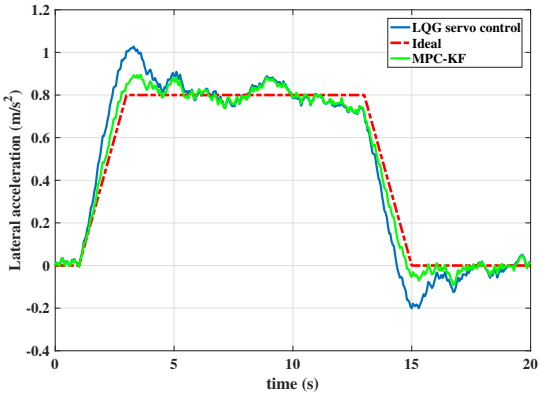

Fig. 19. Carbody lateral acceleration (results with combined deterministic curved track and track irregularities as explained in Subsection 2.3).

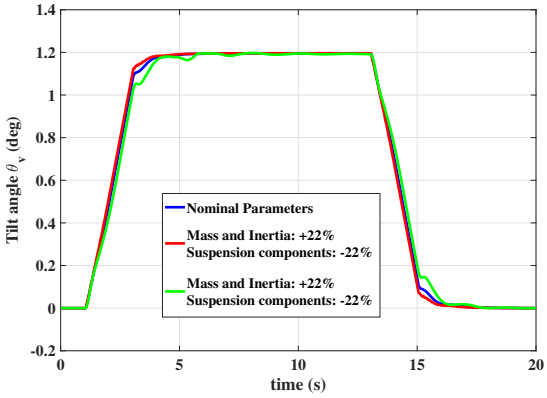

Fig. 21. Response of the MPC-KF in the presence of the parameter uncertainty in the mass, inertia and suspension components.

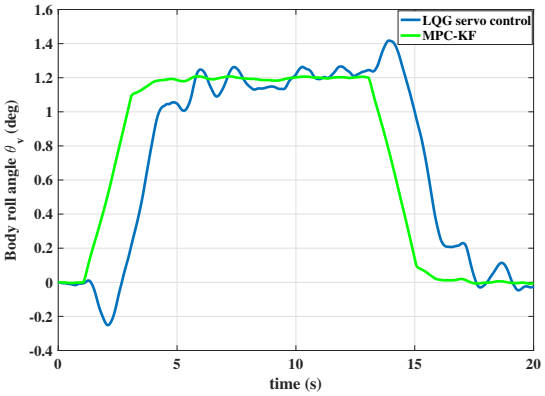

Fig. 20. Carbody roll angle (results with combined deterministic curved track and track irregularities as explained in Subsection 2.3).

spond primarily to deterministic track inputs, while rejecting any track misalignments as much as possible. On the other hand, as shown in Fig. 20, the MPC-KF surpassed the modified LQG control in terms of lower oscillations in the response of the roll body angle.

Here, the robustness of the MPC-KF is evaluated by simulation of the system with modeling errors. The robustness of the control system is quite essential in an actual situation. If the proposed approach has little robustness, the proposed control method is not helpful. An amount of $\pm 22\%$ uncertainty in the inertia and mass parameters is considered in this simulation. Moreover, a $\pm 22\%$ variation in the suspension components (springs, airsprings and dampers) in addition to the aforementioned uncertainty was added to the actual dynamic model. The results (see Fig. 21) show the robust performance provided by the MPC-KF in the case of the presence of parametric uncertainty.

P_{ct} and r.m.s. of lateral acceleration as the factors for ride comfort [6] and also other important details corresponding to the performance of the schemes are compared in Table 4. The control algorithms used as the reference in this table are fundamentally the precedence scheme [31,32], so it is proper to contrast the designed controllers

Table 4. Comfort assessment of various controlling approaches.

Deterministic (as per given units)		PI compensator with a low-pass filter in [31]	PI controller	Estimator-based tilt controller in [32]	Modified LQG controller	MPC-KF
Lateral acceleration	RMS deviation (%g)	1.54	0.133	1.7	0.832	0.142
	Peak value (%g)	12.18	8.491	7.24	9.796	8.287
Roll speed	RMS deviation (rad/s)	0.018	0.033	0.02	0.008	0.002
	Peak value (rad/s)	0.104	0.118	0.1	0.100	0.09
P_{ct} related	Peak jerk level (%g/s)	6.8	4.373	5.17	4.893	5.096
	Standing (% of passengers)	47.62	35.975	29.85	36.412	23.944
	Seated (% of passengers)	13.455	8.397	7.5	9.448	6.289

with the ones mentioned in Table 4. Besides, the proposed algorithm in [32] uses tilting bolster as the actuator, which is nowadays utilized by the majority of tilting body solutions. P_{ct} indicates the percentage of passengers who feel uncomfortable during the negotiation of curve transition. Maximum vehicle body lateral acceleration, maximum lateral jerk, and the maximum carbody roll rate are used to calculate P_{ct}. Table 4 illustrates that the MPC-KF controller outperformed the utilized algorithms in [31] and [32] in terms of ride comfort indices, including the P_{ct} and r.m.s. lateral acceleration i.e., approximately 0.14% and 23.9%, respectively. Moreover, in comparison with other designed controllers in this study, MPC-KF has the best performance in the whole criteria, except the r.m.s. lateral acceleration and peak jerk level. The tracking error of lateral acceleration response in MPC-KF is about 0.01 m/s^2 along the curve. For this reason, PI control obtained a marginal improvement of the r.m.s. lateral acceleration compared to the MPC-KF. The MPC-KF is less effective than the other two controllers in terms of peak jerk level, with 8.29%, due to the abrupt change of slope in the lateral acceleration response at the end of the transition section. This occurrence can be due to the fact that a discrete-time MPC was adopted in this paper. The LQG servo controller results in slightly worse P_{ct} than the other two controllers, owing to the delay in the controller action. Despite the acceptable PI controller performance, due to the aforementioned cause associated with the performance of the BLDC motor, this approach cannot be perceived as an efficient controller to be employed for controlling tilting action. This information was achieved by simulating the control system using these controllers and considering previously mentioned assumptions. Overall, the MPC-KF produces a superb response regarding the performance of the electric actuator, with an outstanding level of ride comfort and reference tracking. However, it is a more complicated and computationally demanding controller than the designed LQG servo controller. It is also seen that the proposed solution for the active tilting train, which uses MPC-KF as the controller, and electrical active anti-roll bar as the actuator exhibits a more satisfying performance in comparison with the method proposed in [32], which uses tilting bolster as a common tilting structure.

5. CONCLUSION

The current research has studied the performance of the tilting trains in curved tracks. According to the fact that the present study has used an anti-roll bar along with an electric motor as the active train actuator, each of them was investigated separately regarding the dynamics governing them. The electric motor used herein is a brushless DC motor. In this study, the proportional-integral approach was employed for the speed controller of the BLDC motor. Besides, this paper focused on a modified LQG control and MPC-KF approach for reducing non-compensated lateral acceleration and improving the actuation system response, especially in the presence of noise. The whole designed controllers are analogous to the 'precedence-type' scheme, with the exception that the tilt command is generated using track data from an onboard track database.

Three various control strategies were performed for the active suspension utilizing a multi-body model railway vehicle. First, a PI control design was used for the active anti-roll bar, and its parameters were selected on the basis of a tuning process. Then, a modified Linear Quadratic Gaussian control system was designed, consisting of the LQI tracker and Kalman filter in order to attain reference tracking and estimation. Subsequently, an MPC controller together with a built-in Kalman filter was applied to the tilting system. The state variables are estimated using the Kalman filter despite the existence of measurement noise. Therefore, the system response is almost devoid of noise. The electrical behavior and performance of the BLDC motor were taken into account in the control system of the tilting railway vehicle and AARB so that the duty fulfillment of the motor could be ensured.

A detailed assessment was carried out based on the torque and current response of the actuator considering three different controllers. As illustrated in the results, the BLDC motor can have a decent and stable performance when the LQG servo and MPC-KF controllers are applied. On the other hand, in the case of using the PI controller, the measurement noise has a negative effect on the control system response and the efficacy of the BLDC motor. In the end, the ride comfort level was evaluated by comparing different controllers. The results indicate that the MPC-KF can also provide significant passenger comfort compared to the LQG servo controller and the algorithms of previous studies.

APPENDIX A: SUPPLEMENTARY MATERIALS

A.1. Airspring model

Disregarding vertical motions and substituting $d_1\theta_r$ for z_r, Fig. 22 shows the airspring model used in the secondary vertical suspension.

$$F_z = -k_{az}(d_1\theta_v - d_1\theta_b) - k_{sz}(d_1\theta_v - d_1\theta_r), \tag{A.1}$$

$$\dot{\theta}_r = -\frac{(k_{sz}+k_{rz})}{c_{rz}}\theta_r + \frac{k_{sz}}{c_{rz}}\theta_v + \frac{k_{rz}}{c_{rz}}\theta_b + \dot{\theta}_b. \tag{A.2}$$

A.2. Notation

y_v, y_b, y_0	Lateral displacement of body, bogie, and track
θ_v, θ_b, δ_a	Roll displacement of body, bogie, and actuator
θ_0, R	Track cant (6 deg), curve radius (1000 km).
θ_r	Airspring reservoir roll deflection
v	Vehicle forward speed, 162 km/h

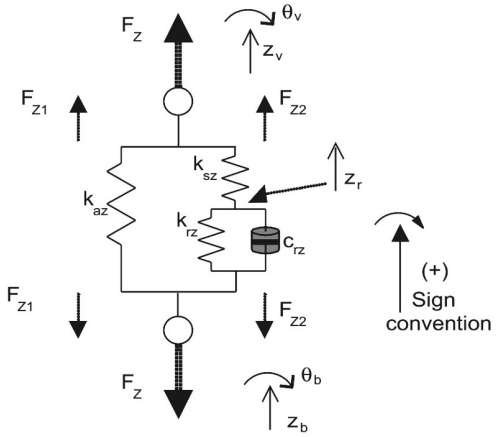

Fig. 22. Airspring model [21].

m_v	Half body mass, 19000 kg
i_{vr}	Half body roll inertia, 25000 kgm^2
m_b	Bogie mass, 2500 kg
i_{br}	Bogie roll inertia, 1500 kgm^2
k_{az}	Airspring area stiffness, 210000 N/m
k_{sz}	Airspring series stiffness, 620000 N/m
k_{rz}	Airspring reservoir stiffness, 244000 N/m
c_{rz}	Airspring reservoir damper, 33000 Ns/m
k_{sy}	Secondary lateral stiffness, 260000 N/m
c_{sy}	Secondary lateral damper, 33000 Ns/m
k_{vr}	Anti-roll bar stiffness/bogie, 2000000 Nm/rad
k_{pz}	Primary vertical stiffness, 2000000 N/m
c_{pz}	Primary vertical damper, 20000 Ns/m
k_{py}	Primary lateral stiffness, 35000000 N/m
c_{py}	Primary lateral damper, 16000 Ns/m
d_1	Airspring semi-spacing, 0.90 m
d_2	Primary vertical suspension semi-spacing, 1.00 m
h_1	Secondary lateral suspension height (body c.o.g), 0.9 m
h_2	Secondary lateral suspension height (bogie c.o.g), 0.25 m
h_3	Height (bogie c.o.g), -0.09 m
h_{g1}	Bogie c.o.g height (rail level), 0.37 m
h_{g2}	Body c.o.g height (rail level), 1.52 m
L_1	Length of anti-roll bar, 2 m
L_2	Arm length of anti-roll bar, 0.7 m
n_r	Reduction ratio of harmonic gearbox, 200

CONFLICT OF INTERESTS

The authors certify that they have NO affiliations with or involvement in any organization or entity with any financial interest or non-financial interest in the subject matter or materials discussed in this manuscript.

REFERENCES

[1] J. T. Pearson, R. M. Goodall, and I. Pratt, "Control system studies of an active anti-roll bar tilt system for railway vehicles," *Proceedings of the Institution of Mechanical Engineers, Part F: Journal of Rail and Rapid Transit*, vol. 212, pp. 43-60, 1998.

[2] A. O. Darlton and M. Marinov, "Suitability of tilting technology to the tyne and wear metro system," *Urban Rail Transit*, vol. 1, pp. 47-68, 2015.

[3] R. Persson, *Tilting Trains: Description and Analysis of the Present Situation*, Royal Institute of Technology, 2007.

[4] E. F. Colombo, E. Di Gialleonardo, A. Facchinetti, and S. Bruni, "Active carbody roll control in railway vehicles using hydraulic actuation," *Control Engineering Practice*, vol. 31, pp. 24-34, 2014.

[5] E. Di Gialleonardo, M. Santelia, S. Bruni, and A. Zolotas, "A simple active carbody roll scheme for hydraulically actuated railway vehicles using internal model control," *ISA Transactions*, vol. 120, pp. 55-69, 2021.

[6] R. Persson, R. M. Goodall, and K. Sasaki, "Carbody tilting–technologies and benefits," *Vehicle System Dynamics*, vol. 47, pp. 949-981, 2009.

[7] R. Zhou, A. Zolotas, and R. Goodall, "Integrated tilt with active lateral secondary suspension control for high speed railway vehicles," *Mechatronics*, vol. 21, pp. 1108-1122, 2011.

[8] H.-Y. Kim, J.-H. Lee, S.-H. Han, N.-J. Lee, B.-T. Kim, and C.-G. Kang, "Experimental study on dynamic load measurement of a tilting mechanism of a railway vehicle using two hydraulic cylinders," *Proceedings of the Institution of Mechanical Engineers, Part F: Journal of Rail and Rapid Transit*, vol. 231, pp. 370-378, 2017.

[9] S. Yim, K. Jeon, and K. Yi, "An investigation into vehicle rollover prevention by coordinated control of active anti-roll bar and electronic stability program," *International Journal of Control, Automation, and Systems*, vol. 10, pp. 275-287, 2012.

[10] V. T. Vu, O. Sename, L. Dugard, and P. Gáspár, "An investigation into the oil leakage effect inside the electronic servo-valve for an $\mathcal{H}_\infty$/LPV active anti-roll bar system," *International Journal of Control, Automation, and Systems*, vol. 17, pp. 2917-2928, 2019.

[11] S. Buma, Y. Ookuma, A. Taneda, K. Suzuki, J.-S. Cho, and M. Kobayashi, "Design and development of electric active stabilizer suspension system," *Journal of System Design and Dynamics*, vol. 4, pp. 61-76, 2010.

[12] R. Goodall, S. Bruni, and A. Facchinetti, "Active control in railway vehicles," *International Journal of Railway Technology*, vol. 1, pp. 57-85, 2012.

[13] B. Fu, R. L. Giossi, R. Persson, S. Stichel, S. Bruni, and R. Goodall, "Active suspension in railway vehicles: A literature survey," *Railway Engineering Science*, vol. 28, pp. 3-35, 2020.

[14] H. Magalhães, P. Antunes, J. Pombo, and J. Ambrósio, "A dedicated control design methodology for improved tilting train performance," *Proc. of the IAVSD International Symposium on Dynamics of Vehicles on Roads and Tracks*, pp. 72-81, 2019.

[15] F. Amirouche, *Fundamentals of Multi-body Dynamics: Theory and Applications*, Springer Science & Business Media, 2007.

[16] F. Hassan, A. Zolotas, and S. M. Shah, "$H\infty$ mixed sensitivity optimization for high speed tilting trains," *Bulletin of Electrical Engineering and Informatics*, vol. 9, pp. 1854-1860, 2020.

[17] F. Hassan, A. C. Zolotas, and T. Smith, "Optimized Ziegler-Nichols based PID control design for tilt suspensions," *Journal of Engineering Science and Technology Review*, vol. 10, no. 5, pp. 17-24, 2017.

[18] A. C. Zolotas, R. Goodall, and G. Halikias, "New control strategies for tilting trains," *Vehicle system dynamics*, vol. 37, pp. 171-182, 2002.

[19] E. Rakhshani, I. M. H. Naveh, H. Mehrjerdi, and K. Pan, "An optimized LQG servo controller design using LQI tracker for VSP-based AC/DC interconnected systems," *International Journal of Electrical Power & Energy Systems*, vol. 129, 106752, 2021.

[20] Y. Jiang, W. Gao, J. Na, D. Zhang, T. T. Hämäläinen, V. Stojanovic, and F. L. Lewis, "Value iteration and adaptive optimal output regulation with assured convergence rate," *Control Engineering Practice*, vol. 121, 105042, 2022.

[21] S. Subchan, A. M. Syafii, T. Asfihani, and D. Adzkiya, "Modified Kalman filter-based model predictive control for ship heading control with probabilistic constraints," *Systems Science & Control Engineering*, vol. 9, pp. 109-116, 2021.

[22] L. Dutta and D. K. Das, "A new adaptive explicit nonlinear model predictive control design for a nonlinear MIMO system: An application to twin rotor MIMO system," *International Journal of Control, Automation, and Systems*, vol. 19, pp. 2406-2419, 2021.

[23] Y. Mizuta, M. Suzumura, and S. Matsumoto, "Ride comfort enhancement and energy efficiency using electric active stabiliser system," *Vehicle System Dynamics*, vol. 48, pp. 1305-1323, 2010.

[24] B. K. Bose, *Power Electronics and AC Drives*, Englewood Cliffs, 1986.

[25] R. Krishnan, *Permanent Magnet Synchronous and Brushless DC Motor Drives*, CRC press, 2017.

[26] A. Zolotas and R. Goodall, *Advanced Control Strategies for Tilting Railway Vehicles*, UKACC Control, 2000.

[27] E. Ostertag, *Mono- and Multivariable Control and Estimation: Linear, Quadratic and LMI Methods*, Springer Science & Business Media, 2011.

[28] S. P. Azad, R. Iravani, and J. E. Tate, "Damping inter-area oscillations based on a model predictive control (MPC) HVDC supplementary controller," *IEEE Transactions on Power Systems*, vol. 28, pp. 3174-3183, 2013.

[29] C. Schmid and L. T. Biegler, "Quadratic programming methods for reduced hessian SQP," *Computers & Chemical Engineering*, vol. 18, pp. 817-832, 1994.

[30] J.-C. Kim, D.-S. Pae, and M.-T. Lim, "Obstacle avoidance path planning based on output constrained model predictive control," *International Journal of Control, Automation, and Systems*, vol. 17, pp. 2850-2861, 2019.

[31] A. C. Zolotas and R. M. Goodall, "Modelling and control of railway vehicle suspensions," *Mathematical Methods for Robust and Nonlinear Control*, pp. 373-411, 2007.

[32] A. C. Zolotas, R. M. Goodall, and G. Halikias, "Recent results in tilt control design and assessment of high-speed railway vehicles," *Proceedings of the Institution of Mechanical Engineers, Part F: Journal of Rail and Rapid Transit*, vol. 221, pp. 291-312, 2007.

Benyamin Anafjeh received his B.S. degree in mechanical engineering from Golpayegan University of Technology, Isfahan, Iran. He received his M.Sc. degree in dynamic and control engineering from the Isfahan University of Technology in 2017. His research interests include control system, robotics, vehicle dynamics & control, multi-rotor drone aircraft control, and estimation theory.

Hassan Moosavi revived his Ph.D. degree in the field of designing and heat transfer from the Mechanical Department of Wichita State University, USA, in May 1990. He is an Associate Professor at Mechanical Engineering Department of Isfahan University of Technology, Iran. His main interested fields are optimization methods, dynamic & robotics, design optimization, metal forming, and thermal mechanics. He has published a book in the area of finite element method and simulation.

Mohammad Danesh received his B.S., M.S., and Ph.D. degrees in control engineering in 1997, 1999, and 2007, respectively, all from Isfahan University of Technology (IUT), Isfahan, Iran. Currently, he is an Associate Professor at the Department of Mechanical Engineering, IUT. His research interests include robotic systems (control, guidance, and navigation), control and stability analysis of dynamical systems, active vibration and acoustic control, and mechatronics.